

Design of a novel localization scheme by combining grid and laser

HONGBIN MA, XINRUI LIU*, QUN HE, YONGSHENG CHEN, JIATENG GUO

College of Resources and Civil Engineering, Northeastern University, Shenyang 110819, P. R. China

We design a novel localization scheme called laser beam scan localization (BLS) by combining grid and light (laser) with mobile localization policy for wireless sensor networks. The scheme utilizes a moving location assistant (LA) with a laser beam, through which the deployed area is scanned. The LA sends IDs to unknown nodes to obtain the locations of sensor nodes. High localization accuracy can be achieved without the aid of expensive hardware on the sensor nodes, as required by other localization systems. The scheme yields significant benefits compared with other localization methods. First, BLS is a distributed and localized scheme, and the LA broadcasts IDs while unknown nodes listen passively. No interactive intersensor communications are involved in this process; thus, sensor energy is saved. Second, BLS reaches a sub-meter localization error. Third, because equation is simple, computational cost is low. Finally, BLS is a low-cost scheme because it does not require any infrastructure or additional hardware for sensor nodes.

(Received December 13, 2011; accepted February 20, 2012)

Keywords: Laser beam, Grid, Localization, Mobile-Assisted localization, Wireless Sensor Networks

1. Introduction

Wireless sensor networks (WSN) consist of numerous small computers equipped with sensors to detect events such as human motion with infrared sensors, or determine the current state of certain variables such as temperature. These sensor nodes are equipped with a radio to communicate with one another and send data to a central computer where the data can be parsed and viewed. Wireless sensor networks extend our capability to explore, monitor, and control the physical world. As a fundamental problem in sensor networks, the self-localization of sensor nodes has recently attracted considerable attention from both academia and industry [1].

Generally, localization algorithms are divided into two categories: range-based and range-free, according to the need to measure the range between nodes. The former is defined by protocols that use absolute point-to-point distance estimates or angle estimates to calculate location and adopt trilateration-based methods, triangulation-based methods, or maximum-likelihood estimators. Range-based algorithms can obtain higher precision, and typical approaches include DV-Distance [2], MDS-MAP [3], and Malguki [4]. However, the cost and the limitations of the hardware based on sensing nodes prevent the use of range-based localization schemes that depend on absolute point-to-point distance estimates. Coarse accuracy is sufficient for most sensor network applications; thus, solutions in range-free localization are being pursued as a cost-effective alternative to more expensive range-based approaches. Many range-free localization schemes, such as the

bounding box [5], convex position [6], APIT, Centroid, DV-Hop, and Amorphous [7], have been proposed. Most of these schemes estimate the location of sensor nodes by exploiting radio connectivity information among neighboring nodes. They eliminate the need for high-cost specialized hardware. The trade-off, however, is less accurate localization. Few methods take advantage of both types, as does ROCRSSI [8].

Research on range-free localization based on RSSI is very popular. Localization based on received signal strength has been studied extensively in [9], [10], [13], and [14]. However, sub-meter localization precision is difficult to achieve because of changes in temperature, obstacles, transmission mode, and other varied changes in environmental conditions.

In summary, most studies on sensor positioning exploit distance or angle measurements from anchor nodes or neighbors. They have become a subset of the geometric graph-embedding problem or a constrained optimization problem. Obtaining the optimal solution (estimated locations) in the context of sensor networks, however, is challenging [1]. Trade-offs among accuracy, computation and communication overhead, scalability, and other issues must be addressed.

To overcome these limitations, we present a localization system, called laser beam scan localization (BLS), for WSN. Our system requires line of sight between a single device and the sensor nodes, as well as a map of the terrain where the sensor field is located. According to a certain gap, the location-assistant (LA) scans the deployed region through the laser beam and sends the corresponding ID to unknown nodes. An unknown node can calculate its position only by

scanning gap. The starting position of the deployed region and received ID. As well as precision can be arrived at by sub-meter. Based on this idea, we propose four localization modes rooted in two categories. The first is BLS-IA (LA's scan in the deployed region) categorized further into 'row-column scanning' and 'only one row/column scanning' modes. The other category is BLS-OA (whirling laser beam scanning out of the deployed region), subdivided to 'whirling fixed width of laser beam scanning' and 'swing spot of laser to construct laser beam scanning' modes.

In this paper, four modes are analyzed, simulated, and implemented, and four positioning mode features in BLS are compared. The theory analysis, simulation, and experiment demonstrate the effectiveness and advantages of BLS.

The rest of this paper is organized as follows: the next section summarizes related work; Section 3 introduces the principle of BLS as well as the simulation and experiment on the system; Section IV explains light localization issues, and Section V presents the conclusion.

$$[\max(x_i - r), \max(y_i - r)] * [\min(x_i + r), \min(y_i + r)], i = 1, 2, \dots, k \quad (1)$$

The bounding box algorithm is very simple and incurs low communication cost. Its main shortcoming is its demand for a higher density of anchors.

He et al. [7] proposed an area-based APIT algorithm. In the APIT scheme, the point-in-triangulation test is performed. In this test, a node chooses three anchors from all audible anchors (anchors from which a beacon is received) and tests whether it is inside the triangle formed by connecting these three anchors. APIT repeats the point-in-triangulation test with different audible anchor combinations until all combinations are exhausted or the required accuracy is achieved.

The laser beam localization scheme for WSN is rarely discussed in current literature. In [15], a localization system called Spotlight was presented. The system employs an asymmetric architecture, in which sensor nodes do not need any additional hardware other than what they currently have. All the sophisticated hardware and computation reside on a single Spotlight device, which uses a steerable laser light source, illuminating the sensor nodes placed within a known terrain. It uses the spatio-temporal properties of well controlled events in the network (e.g., light) to obtain the locations of sensor nodes and sub-meter localization error. However, time-synchronization protocol is required, increasing system complexity.

In [20], location-guided laser beams are projected to the centers of grid cells to trigger sensors within one hop of a communication range to form sensor clusters in the virtual grid. In the system, laser beams are used to guide sensor clusters to the local position.

Many approaches to mobile localization have been

2. Related work

References [5,11,16], etc. are based on the grid localization algorithm. In [5], Simić and Sastry constructed a bounding box, which is a distributed algorithm for node localization in a discrete model of a random ad hoc communication network. The expected value of estimated position A_s , and the probability that $A_s=1$ cell were computed. The algorithm for each unknown node S is as follows.

Let S be a random node whose position is unknown in square area D , and (x_i, y_i) coordinates of S . Area D is divided into n^2 grids. The radius of the communication radio is referred to as the number of unit ρ . A node's communication region is $2\rho \times 2\rho$.

Step A. Information about the positions of the known neighbors of S is gathered.

Step B. An estimate of the position of S is computed using (1), expressed as

proposed [1,12,17,18,19,21]. In [1], the authors utilized a moving LA with a global positioning system or a predefined moving path to help location-unaware sensors accurately discover positions. Each sensor collects the location beacons, measures the distance between itself and the LA based on the received signal strength, and individually calculates the locations via an algorithm based on the Unscented Kalman Filter (UKF). Unknown node costs increase because the UKF algorithm is used and the iteration method is applied.

Xiao [21] presented a distributed method for localization of sensor nodes using a single moving beacon, in which sensor nodes estimate their position based on the range-free technique. The author proposed the beacon as having three movement patterns (SSL, DSL, and random movement pattern), and used a random value to present the variance of path loss. This random value (Rand) follows a Weibull distribution. After the RSSI signal is adjusted, the estimation precision arrives at the sub-meter. However, the load of the scheme increases.

3. BLS Scheme

The principle of BLS has the following characteristics:

- It uses a mobile-assisted LA.
- The LA is equipped with a laser beam.
- The laser beam constructs a grid and the LA scans the deployed area, so the whole deployed area is divided by the laser beam grid and LA sends the ID corresponding to every grid.
- Every unknown node utilizes the ID and gap count to

estimate unknown node positions.

1. BLS-IA

The deployed area where LA scans unknown nodes based on BLS is defined by BLS-IA.

1.1. 'ROW-COLUMN SCANNING' MODE

Figure 1 shows a schematic of the principle of 'row-column scanning' mode. In Fig.1, the deployed area is Length*Length and starting coordinate is defined as (0, 0). The width of the laser beam is denoted by "gap." In Fig.1, we can assume that LA scanning y axis is a sample. The LA, with the laser beam, scans one column (y axis) in the area from the starting coordinate across every "mgap," ("mgap" is the short step of LA movement across y or x axis.). The LA sends the ID to the unknown node corresponding to the row number before it scans one row (x axis). To ensure that the light is received by all unknown nodes in the area, the "mgap" value should be less than or equal to the "gap" value. Here it is noted that the photosensitive devices devised in the every unknown node are used to receive illumination of the laser beam and the unknown node receives ID send by wireless signal as soon as its photosensitive devices receive illumination of the laser beam.

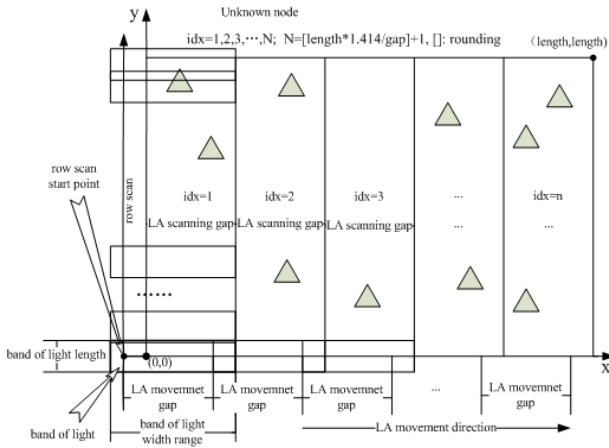


Fig. 1. Schematic of principle of the 'row-column scanning' mode.

The implementation of 'row-column scanning' mode can be divided into three stages:

(1) A mobile LA (aircraft, balloon, robot, vehicle, etc.) is equipped with the laser beam. The width is the "gap" that projects light in the deployed area of the unknown nodes. Then, LA begins to scan the area from the area zeros along the x axis and moves one "mgap" after it scans one row and sends the ID of the row to the unknown node. The LA scans the area along the y axis in a similar manner.

(2) The unknown node use the newest ID to update the older ID and calculate their positions only if it receive light.

(3) The deployed area grids are constructed through row and column scans. The center coordinates of every grid are used as the coordinates of the unknown node in the grid. The estimation coordinates (\hat{x}, \hat{y}) can be described as

$$\begin{cases} \hat{x} = x_0 + mgap * (x_{id} - 0.5); & x_{id} = 1, 2, 3 \dots n \\ \hat{y} = y_0 + mgap * (y_{id} - 0.5); & y_{id} = 1, 2, 3 \dots n \end{cases}, (mgap \leq gap) \quad (2)$$

where (x_0, y_0) represents the starting point of row and column scans. In (2), the "mgap" is the LA movement gap along a row or column. The x and y axes IDs received by the nodes are represented by x_{id} and y_{id} . To ensure that all nodes receive light, the mgap value must be less than or equal to the gap value.

1.2. 'ONLY ONE ROW/COLUMN SCANNING' MODE

The 'only one row/column scanning' mode is based on 'row-column scanning' mode, but differs from the latter in the following aspects:

When the LA scans the area along the row, the LA sends x and y axes IDs simultaneously as it moves every gap distance. Therefore, the LA needs to scan only the area along the x or y axis. The localization duration is cut in half compared with 'row-column scanning' mode. However, controlling the LA in the 'only one row/column scanning' mode is complex.

2. BLS-OA

The LA device of BLS-IA is simple. However, because light scanning is in the deployed region, laying out vehicle, cable, etc., moving the LA indoors may become complex. In addition, the functionality of this mode may be limited in military and special environments.

Based on the abovementioned reasons, we propose BLS-OA in this paper and subdivide it into 'whirling fixed width of laser beam scanning' and the 'swing spot of laser to construct laser beam scanning' modes. The 'whirling fixed width of laser beam scanning' mode uses a fixed laser beam, whereas the 'swing spot of laser to construct laser beam scanning' mode utilizes a swing point laser to form the laser beam. Both modes turn bands of light out of the region to scan the region and use a wireless module to send IDs to unknown nodes. Finally, the unknown node calculates estimation coordinates using the ID and other parameters.

Under BLS-OA, several issues are considered: (1) The estimation precision drops sharply when the laser beam widens because light-projected distance increases as a result of light scattering. (2) The angle at which the laser beam is projected affects the response of photosensitive devices. Therefore, localization coverage is affected. (3) Demand accuracy of adjusting the laser beam increases as the LA rises. The deployed region becomes larger; if not, estimation precision deteriorates.

We considered using laser to resolve the first issue

because the 0.5 mw to 5 mw scattering angle of the semiconductor laser source is only 0.001 to 0.0001 radian.

Two solutions were proposed to address the second issue: one is to use a large power laser source and the other is to employ multi-photosensitive chips to form a photographic spherical body. This way, Omni directional light scanning can be received. However, the degree of differentiation of photosensitive chips increases.

In resolving the third issue, we proposed using a micro stepping controller to control the stepper motor. The step angle can reach a level of below 0.1.

3. ALGORITHM ANALYSIS

3.1. Ideal Estimation Errors

The algorithm analysis is based on the 'row-column scanning' mode (the features of the other three modes are similar to the 'row-column scanning' mode). Given the idea that the laser beam width does not fluctuate and LA movement has no error, we assume that in a square region, $Q = [0, L]' [0, L]$ m², called the unknown node deployed area. We randomly scatter N nodes, each

$$E(\text{location-err}) = \dot{\theta}_0^{\text{gap}} \dot{\theta}_0^{\text{gap}} \frac{1}{m \text{gap}^2} \sqrt{(x - \frac{m \text{gap}}{2})^2 + (y - \frac{m \text{gap}}{2})^2} dx dy = \frac{1}{6} [\sqrt{2} + \ln(\sqrt{2} + 1)] m \text{gap} \gg 0.3826 * m \text{gap} \quad (4)$$

From (4) and under ideal conditions, the precision of the 'row-column scanning' mode (including that of other modes) is similar and in direct proportion to the LA gap value and has nothing to do with other parameters.

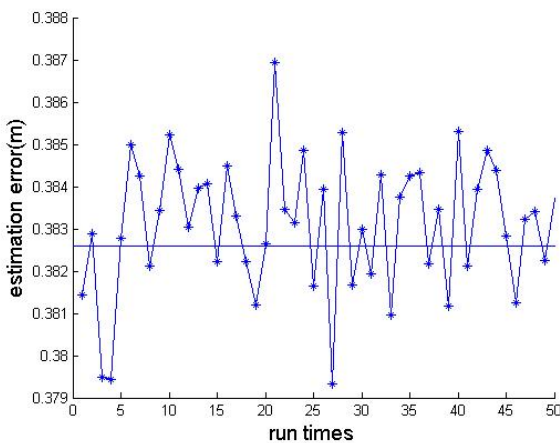


Fig. 2. Estimation error (nodes=100) under ideal conditions.

For simulation settings, we consider a typical 2D network of 100 unknown nodes randomly deployed within a 200×200 m² field. The laser beam width (W) is 1m and LA movement gap (i.e. “mgap”) is 1m. The experimental results reported in this paper are the

of which is equipped with an RF transceiver and photosensitive devices. Given that the row scan gap and column scan gap are “mgap” meters and LA starts scanning the area from Q’s (0, 0), the localization estimation error is given as follows.

The node is deployed in Q according to uniform distribution; thus, the distribution probabilities of every unknown node in the grid, formed by row and column scans, are equal. Therefore, the estimation error in the area can be calculated in a grid.

Let grid $G = [0, m \text{gap}]' [0, m \text{gap}]$ m². In any unknown node i, coordinate (x, y) is uniformly deployed in G. Then, the two-dimensional probability density function of the node is $1/m \text{gap}^2$. Given that the center of grid coordinates (0.5 mgap, 0.5 mgap) are seen as the estimation coordinates, the localization error of node i is defined by

$$\text{location-err} = \sqrt{(x - 0.5 m \text{gap})^2 + (y - 0.5 m \text{gap})^2} \quad (3)$$

Then, the localization error [E (location-err)] in Q can be presented as

median of 100 runs. Fig. 2 shows that the estimation error fluctuates from minimal 0.379 m to maximal 0.387 m around the ideal error 0.3826 m.

3.2. Analysis of BLS Estimation Error with Varying Laser beam

In the 'row-column scanning' mode (the features of other modes are similar to this mode), we assume that the difference between the grid region constructed by light scanning and the ideal grid region including grid length and width alteration stimulates errors and enables both length and width error values to be “gaperr” [called light error]. The value of the laser beam width is “gap.” In addition, the LA movement gap value in row and column scanning is “mgap,” and movement gaps are not errors. If they exist as errors, they are called movement errors.

Four grid partitions (Fig. 3) under laser beam fluctuation are created based on the abovementioned conditions. Four actual black and thick grid centers are used in four localization estimation coordinates. The four dashed grids are composed of left, right, bottom, and top dotted lines. The left dotted line represents the light band boundary of the last time row scanning was performed and the bottom dotted line is the light band boundary of the last column scanning. Meanwhile, the right and top dotted lines indicate current row and column light scanning boundaries, respectively. The four dashed grids are actual unknown nodes in

deployed regions that use estimate coordinates of four actual line grid centers. Figure 3a presents no estimation error grid. In this situation, the theoretical value of the estimation error is 0.3826 mgap . Fig. 3b shows every edge of the grid projected by light existing error, including the statuses of the other three modes. Fig. 3c shows that in the last row and column scanning, the two edges have maximal error, whereas in the current row and column scanning, the other two edges have minimal error. Under the conditions in Fig. 3c, the maximal estimation error is defined as $\frac{\sqrt{2}}{2}(\text{mgap} - \text{gap} \times \text{gaperr})$. In Fig. 3d, the error condition of the edge is opposite that in Fig. 3c. Therefore, the maximal estimation error is $\frac{\sqrt{2}}{2}(\text{mgap} + \text{gap} \times \text{gaperr})$.

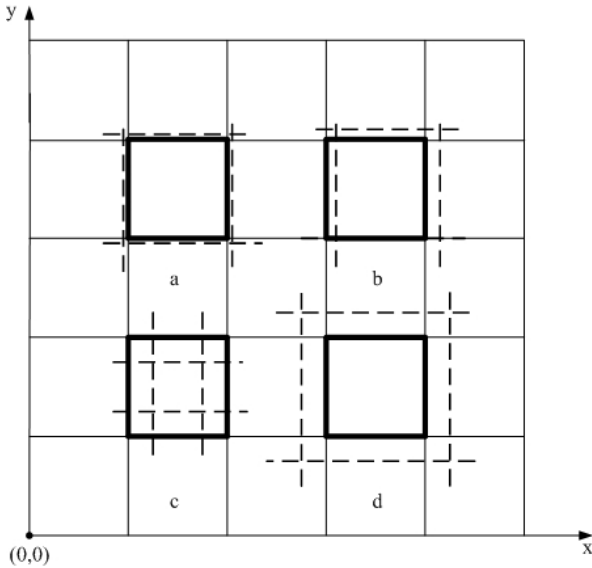


Fig. 3. Grid partition based on band of light width variations.

From the analysis above, we conclude that $\frac{\sqrt{2}}{2}(\text{mgap} + \text{gap} \times \text{gaperr})$ is the maximal estimation error under varying conditions of the laser beam width. On the other hand, in the ideal condition, the maximal estimation error is $\frac{\sqrt{2}}{2} \text{mgap}$. We can assume that the specific value between the former and the ideal condition's maximal estimation error is K , as defined by (5). Error incremental KI under varying conditions of the laser beam width is described in (6).

$$K = \frac{\frac{\sqrt{2}}{2}(\text{mgap} + \text{gap} \times \text{gaperr})}{\frac{\sqrt{2}}{2} \text{mgap}} = 1 + \frac{\text{gap} \times \text{gaperr}}{\text{mgap}}, (\text{mgap} \leq \text{gap}) \quad (5)$$

$$KI = K - 1 = \frac{\text{gap} \times \text{gaperr}}{\text{mgap}}, (\text{mgap} \leq \text{gap}) \quad (6)$$

Equation (6) shows that KI is inversely proportional to the “mgap” value and is directly proportional to “gap×gaperr” values. When, “gap or mgap” is constant, the relationship between KI and “gaperr” is linear. If “gaperr” is unchanged, KI arrives at a minimum when “gap” value is equal to “mgap” value.

3.3. Relationship between Adjusting the Gap of the Laser beam and its Movement

In a square region, $Q = [0, L] \times [0, L] \text{ m}^2$; we assume that the height of LA $H \text{ m}$ (the vertical distance between the laser band and the unknown node) and the scanning gap generated by adjusting the band is set to “gap” m ; the laser beam width is defined by $W \text{ m}$, and $W = \text{gap}$. Given the length of laser beam ‘LL’ m and that ‘LL’ is much less than the gap value, we consider that $LL \ll \text{gap}$, the widening of the laser beam can be ignored. In addition, the movement gap of the LA is defined by “mgap” m ; thus, we let $\text{mgap} = \text{gap}$. On this scenario, the theoretical estimation error is 0.3826 mgap and the maximal ideal estimation error is 0.707 mgap .

The relationship between the rotation angle and the scanning gap under the abovementioned conditions are shown in Fig. 4.

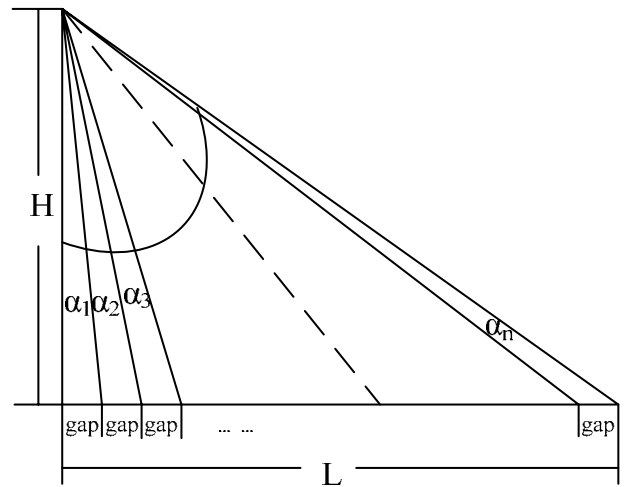


Fig. 4. Relationship between rotation angle and scanning gap.

In Fig. 4, H is the vertical distance between the laser band and the unknown node. The edge of region Q is L . The rotation angle when scanning "gap" is represented by $\alpha_1, \alpha_2, \alpha_3, \dots, \alpha_n$, and $\alpha = \arctan(L/H)$. The number of gaps is denoted by $GAPC = \lceil L/gap \rceil + 1$, and $\lceil \cdot \rceil$ indicates rounding operation. Therefore, the rotation angle of every "gap" α_i can be defined by (7). The smaller α_i is, the longer L becomes.

$$\alpha_i = \arctan\left(\frac{i \cdot gap}{H}\right) - \arctan\left(\frac{(i-1) \cdot gap}{H}\right), i = 1, 2, \dots, GAPC \quad (7)$$

3.4. Laser beam Width and Length Varied by Light Scattering

If the laser divergence angle is β radian and assuming LL 's width can be one line, the laser beam width and length variation by light scattering is defined by (8).

$$LL_{\alpha_i} = H \times \tan\left(\arctan\left(\frac{i \cdot gap}{H}\right) + b\right) - i \cdot gap, i = 1, 2, \dots, GAPC \quad (8)$$

The increment of the laser beam caused by β scattering after the α_i turns is LL_{α_i} . If $\beta \gg 0$ exists, then $\tan \beta \approx \beta$ can be obtained. Equation (8) can be simplified to (9).

$$LL_{\alpha_i} \approx (H^2 + i^2 \cdot gap^2) \times \frac{b}{H - (i \cdot gap)b}, i = 1, 2, \dots, GAPC \quad (9)$$

In (9), if H , i , and gap values are constant, β becomes greater and LL_{α_i} increase is faster than linear increase.

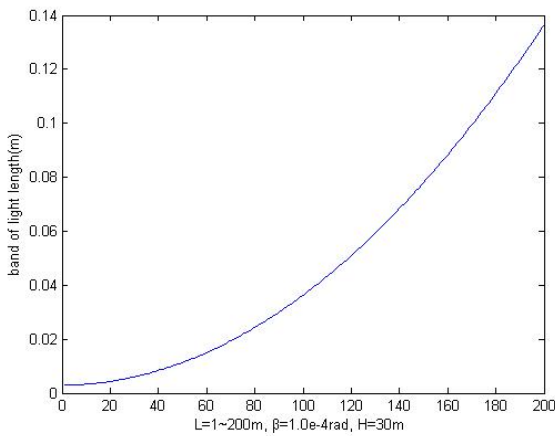


Fig. 5. Bands of light length varied by optical path increase.

To further show this relationship, we assume that $H=30$ m, $n=1-200$ (i.e., the deployed region from $1 \text{ m} \times 1$

m to $200 \text{ m} \times 200 \text{ m}$), rotation gap is 1 m , and the laser divergence angle β is 1.0×10^{-4} radian. The laser beam length varied by optical path increase is shown in Fig. 5.

Fig. 6 shows that although L is up to 200 m , the laser beam length is only 0.14 m .

The laser beam width increment varied by light scattering LW_{α_i} is described by (10). Figure 6 also shows the principle of the laser beam width increment.

$$LW_{\alpha_i} = La_i' \times \tan b = \frac{H}{\cos\left(\sum_{m=1}^i \alpha_m\right)} \times \tan b, i = 1, 2, \dots, GAPC \quad (10)$$

In Fig. 6 and (10), α_i is defined by (7). The optical path when LA turns to α_i is La_i' . Other symbols are defined in section III 3.3.

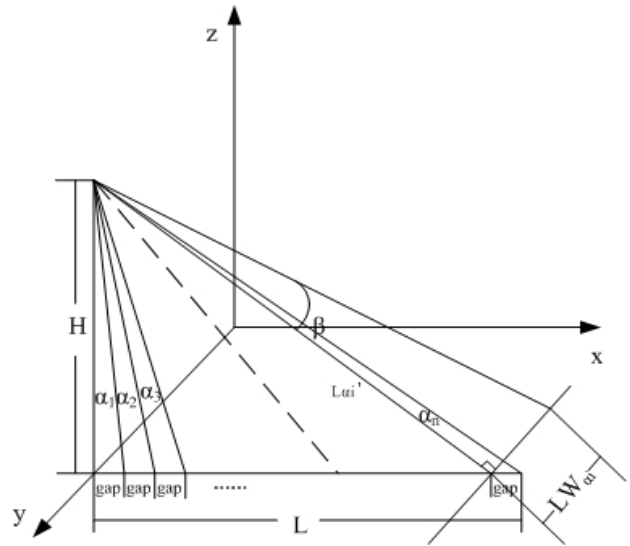


Fig. 6. Principle of the band of light width increment.

Compared with the laser beam length increment, the laser beam width increment is smaller. Therefore, we conclude that the localization estimation precision, which reaches the sub-meter in the large region, is not vulnerable to optical path change.

4. BLS Duration

We assume that the LA movement speed is $V \text{ m/s}$, localization duration is t seconds, and unknown node calculation time is ignored.

Under the 'row-column scanning' mode, localization duration is defined by (11) and $\lceil \cdot \rceil$ is the rounding process.

$$t = 2 \times \frac{L}{V} \times \left(\left[\frac{L}{mgap} \right] + 1 \right) \quad (11)$$

Under the ‘only one row/column scanning’ mode, localization duration t is expressed in (12).

$$t = \frac{L}{V} \times \left(\left[\frac{L}{mgap} \right] + 1 \right) + \frac{L}{V} = \frac{L}{V} \times \left(\left[\frac{L}{mgap} \right] + 2 \right) \quad (12)$$

In the ‘whirling fixed width of laser beam scanning’ mode, given rotation speed V' (rad/s) and LA scans L (m), the distance when it rotates is L' (rad). We can see that L' does not exceed $\pi/2$. However, rotation time is generally dependent on the sensitivity and response ability of the photosensitive chip. For simplicity, we ignored L'/V' . Therefore, localization duration t is (13) under the ‘whirling fixed width of laser beam scanning’ mode.

$$t = \frac{L}{V} \times \left(\left[\frac{L}{mgap} \right] + 1 \right) + \frac{L'}{V'} \gg \frac{L}{V} \times \left(\left[\frac{L}{mgap} \right] + 1 \right) \quad (13)$$

In the ‘swing spot of laser to construct laser beam scanning’ mode, the time spent in swinging the laser depends on swing speed, laser power, laser spot size, photosensitive performance, rotation speed, and so on. When swing and rotation are simultaneous, localization duration is expressed as (13) under the ‘swing spot of laser to construct laser beam scanning’ mode.

From (11), (12), and (13), we conclude that duration is longest under the ‘row-column scanning’ mode and is twice as much as that in the other modes. The duration is shortest under BLS-OA. The duration of BLS scheme is about a dozen or so minutes in the large scene (100 m×100 m field).

5. Cost Function

The relationship among localization precision (r), scanning speed (V), region size (edge L), and duration (t) is called cost function. Equation 13 can be substituted into (4) to yield

$$r = K_1 \times 0.3826 \times \frac{L^2}{Vt - K_2 \times L} \quad (14)$$

If $K_1=2$ and $K_2=1$ are used, (14) is used in the ‘row-column scanning’ mode. If $K_1=1$ and $K_2=2$ are set, (14) is applied to the ‘only one row/column scanning’ mode. When $K_1=K_2=1$, (14) is used in BLS-OA. In (14), r is dependent on L , V , and t . The applications need to consider the trade-off.

4. Experiment and Analysis for BLS Scheme

4.1. Experiment and Analysis based on BLS-IA

4.1.1. The ‘row-column scanning’ mode Experiment

Experimental scenario: The 3 m×3 m shelf is fixed in a 4 m×3 m room. LA distance is 0.5 m from the ground. The LED spotlight spot range on the ground is greater than 20 cm, and we assume that a 15 cm spot diameter is valid for the phototransistor. The phototransistor is a 3DU11 model, collector resistance is 2 k, and voltage is 3.3 V. The mobile platform is defined as the platform on which the LA moves. The seven unknown nodes are deployed on the region 150 cm×150 cm.

Experiment hardware and software: The wireless location network based on the Zigbee protocol is composed of nine wireless homemade Zigbee nodes with CC2430. One of the nodes acts as a sink connected to a laptop through a serial line. The sink is responsible for sending control parameters to the LA and receiving location positions. The other node serves as LA’s wireless communication module. Aside from the wireless communication module, a mobile vehicle and LED spotlight compose the LA. The other seven nodes equipped with the phototransistor are unknown nodes.

In Table 1, the average experimental estimation is 10.6 cm. At the same time, the theoretical maximal error is $\frac{\sqrt{2}}{2} mgap = \frac{\sqrt{2}}{2} \times 15cm = 10.6cm$. When the unknown nodes are deployed on the edge of the region, the average experimental estimation error is equal to the theoretical maximal error. Another experimental scenario is the deployment of unknown nodes near the region. The result of this scenario is shown in Table 2, and Fig. 5 is the experimental site photo.

Table 1. Experiment result under the ‘row-column scanning’ mode.

No.	physical position cm)	experimental estimation position (cm)	experimental estimation error (cm)
1	X=0,Y=0	X=7.5,Y=7.5	10.6
2	X=150,Y=0	X=157.5,Y=7.5	10.6
3	X=0,Y=75	X=7.5,Y=82.5	10.6
4	X=150, Y=75	X=157.5,Y=82.5	10.6
5	X=0,Y=150	X=7.5,Y=142.5	10.6
6	X=150,Y=150	X=157.5,Y=142.5	10.6
7	X=75,Y=75	X=82.5,Y=82.5	10.6
experimental average estimation error=10.6cm			

Table 2 shows that the experiment and simulation results are concordant with the theoretical analysis on the 'row-column scanning' mode. Localization precision achieves centimeter level.

Table 2. Result (nodes nearly) under the 'row-column scanning' mode.

No.	physical position (x,y) cm	experimental estimation position (x,y)cm	simulation estimation position (x,y) cm (light error =20% movement error =3%)
1	0,0	7.5,7.5	7.5,7.5
2	75,0	67.5,7.5	82.5,7.5
3	150,0	142.5,7.5	142.5,7.5
4	37.5,37.5	37.5,37.5	37.5,37.5
5	112.5,37.5	112.5,37.5	112.5,37.5
6	0,75	7.5,82.5	7.5,67.5
7	150,75	142.5,82.5	142.5,67.5
8	37.5,112.5	37.5,127.5	37.5,112.5
9	112.5,112.5	97.5,127.5	112.5,112.5
10	0,150	7.5,157.5	7.5,157.5
11	75,150	67.5,157.5	67.5,157.5
12	150,150	147.5,157.5	142.5,157.5
13	75,75	67.5,82.5	67.5,67.5
experimental average estimation error=9.9cm, simulation average estimation error (100 runs)=7.3cm			

1.2. The 'only one row/column scanning' mode experiment

Experimental scenario: Thirteen unknown nodes are deployed in a 150 cm×150 cm square region. Other configurations are the same as those of the 'row-column scanning' mode experiment.

Experimental result and analysis: Table 3 shows that the experimental estimation error is greater than the simulation estimation error. This is because actual circumstances and devices are more complex compared with simulations. However, the experimental estimation error is lower than the theoretical value. As expected, precision levels in 'only one row/column scanning' and 'row-column scanning' modes are similar.

Table 3. Results under the 'only one row/column scanning' mode.

No.	physical position (x,y) cm	experimental estimation position (x,y)cm	simulation estimation position(x,y) cm (Light error =20% movement error =3%)
1	0,0	7.5,7.5	7.5,7.5
2	10,20	7.5,22.5	7.5,22.5
3	30,75	37.5,82.5	22.5,82.5
4	90,75	97.5,82.5	97.5,82.5
5	90, 82	97.5,97.5	82.5,82.5
6	130,125	142.5,127.5	127.5,127.5
7	75,135	82.5,142.5	82.5,127.5
experimental average estimation error=10.6cm, simulation average estimation error (100 runs)=8.14cm			

2. Simulation and Experiment based on BLS-OA

2.1. The 'whirling fixed width of laser beam scanning' mode Simulation

The implementation of the gap width light source with a small scattering angle line is the key in the 'whirling fixed width of laser beam scanning' mode. One of the methods to construct this is to use multi-spot spot lasers that are parallel to each other.

To simulate the 'whirling fixed width of laser beam scanning' mode, MATLAB was used. To show the performance of the proposed the 'whirling fixed width of laser beam scanning' mode, a typical 2D network of 10 to 200 nodes randomly deployed within a 200 m×200 m field was considered. The simulation results reported are from 100 runs. We used values of $\beta=1.0 \times 10^{-4}$, $H=30$ m, $W=1$ m, $mgap=1$ m, $gap=1$ m in our experiments.

Fig. 7 shows the estimation error varied by the number of nodes in the 'whirling fixed width of laser beam scanning' mode. The localization error falls between the ideal and maximal errors, having a value of about 0.63 m.

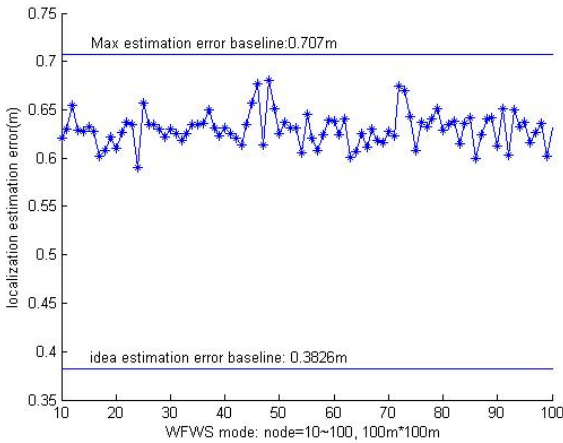


Fig. 7. Estimation error varied by the number of nodes.

$$y=0.01 \times A \sin(2 \times x \times p) + ((0.8 + 0.2 \times \text{randn}(1)) \times A) \times \sin(0.01 \times \frac{(x + \text{randn}(1) \times W)}{W} \times 2 \times p) \quad (15)$$

5. Result and Analysis

Experimental and simulation results under the ‘swing spot of laser to construct laser beam scanning’ mode are shown in Table 4.

Table 4. Results under the ‘swing spot of laser to construct laser beam scanning’ mode.

NN	physical position (x,y) cm	experimental estimation position (x,y)cm	experimental average estimation error =12.7(cm)
1	0,0	7.5,7.5	
2	75,0	67.5,7.5	
3	150,0	142.5,7.5	
4	37.5,37.5	37.5,52.5	
5	112.5,37.5	97.5,52.5	
6	0,75	7.5,82.5	
7	150,75	142.5,82.5	
8	37.5,112.5	37.5,127.5	
9	112.5,112.5	97.5,127.5	
10	0,150	7.5,157.5	
11	75,150	67.5,157.5	
12	150,150	147.5,157.5	
13	75,75	67.5,82.5	

The experiment results show that the experimental average estimation error is larger than the ideal maximal error (10.6 cm) because the extended laser beam width exceeds the theoretical value when the mechanism of the LA device vibrates and swings. Thus, the LA under the ‘swing spot of laser to construct laser beam scanning’ mode needs a high machinery

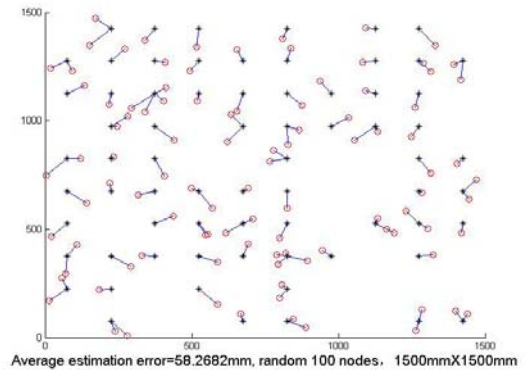
2.2. Experiment and Analysis under the ‘swing spot of laser to construct laser beam scanning’ Mode

The experiment scenario is similar to that of the ‘only one row/column scanning’ mode. In addition, the monitor node added to the Zigbee network supervises the status of unknown nodes receiving IDs.

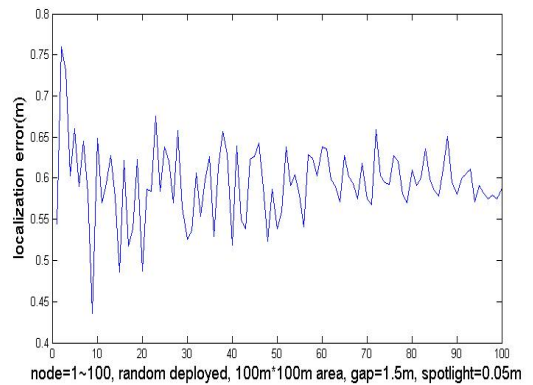
The Laser beam Generating Experiment and Simulation Functions

The large number of experiments indicates that the shape of the laser beam approximates sine fluctuation with high harmonics. Hence, we use (15) to simulate the laser beam. In (15), randn(1) refers to N(0, 1), A is Amplitude, and W is the laser beam width. The simulation is shown in Fig. 8.

production process.



(a) Simulation in small region



(b) Simulation in large region

Fig. 8. Simulation under the ‘swing spot of laser to construct band of light scanning’ mode.

We used MATLAB to simulate the ‘swing spot of

laser to construct laser beam scanning' mode, which is divided into small and large scenarios. In the small scenarios, we considered a 2D network of 100 nodes randomly deployed within a 1500 mm×1500 mm square region. Values of the laser beam used are width=15 cm, length=15 cm, and laser spot diameter=0.5 cm. Results (100 runs) are shown in Fig. 8(a). In the large scenario, the deployed region is 100 m×100 m and values used

are laser beam width=1 m and laser spot diameter=5 cm. Fig. 8(b) shows the results which are concordant with the theoretical analysis

3. Four Positioning Mode Features in BLS

In Table 5, comparison of four positioning mode features in BLS is shown.

Table 5. Comparison of four positioning mode features in BLS.

Mode Parameters	'row-column scanning'	'only one row/column scanning'	'whirling fixed width of band of light scanning'	'swing spot of laser to construct band of light scanning'
Duration	Max	Normal	Min	Min
Category	BLS-IA		BLS-OA	
LA complexity	Simple	Normal	Hard	Hard
Localization precision impact by device	Small	Smaller	Bigger	Big
Demand of LA wireless range	Small		Big	
Flexibility	Small	Smaller	Bigger	Big
Scope of application environment	Small	Small	Big	Big

6. Light localization

Based on light localization, the proposed system requires line of sight between a single device and the sensor nodes; the photosensitive chip is subject to ambient light, and so on. Light localization is suspected because of these unfavorable factors. However, light localization can be applied to numerous scenarios such as indoor, night, and non-sunny day situations. In a sunny day scenario, using an optical filter on top of the photosensitive sensor is the solution to the problem. In particular, WBLS-OA without deployed region scanning and localization increases the range of applications. In addition, infrared laser emitting in the range [750, 1000] nm can be considered for stealth.

7. Conclusions

We presented the design, implementation, and evaluation of a localization system for WSN called BLS. The basic idea is to reach sub-meter precision and low cost of a node by using grid and light (laser) with mobile localization policy for wireless sensor networks. The moving behavior of the LA is an important aspect for localization performances. This system is divided into four modes: 'row-column scanning' mode, 'only one row/column scanning', 'whirling fixed width of laser beam scanning', and 'swing spot of laser to construct laser beam scanning' according to LA's moving fashion. In a real environment and simulation,

four light localization modes are described. The experiment results illustrate that four light localization modes are valid and effective in their specific application environments. As to future work, the accuracy of the system can be further improved by iteration scanning. Improving scheme localization duration is another area for future exploration.

Acknowledgements

The authors would like to acknowledge the financial support from the National Natural Science Fund Project of China (41001228).

References

- [1] L.Q. Zhang, Q. Cheng, Y.G. Wang, and S. Zeadally, IEEE Transactions On Computers, 2008, pp. 246–260.
- [2] B. N. Dragos Niculescu, "Ad Hoc Positioning System (APS)," Proc. IEEE INFOCOM'03, 2003.
- [3] W. R. Yi Shang, Y. Zhang, M. Fromherz, "Localization from Mere Connectivity," Proc. IEEE ACM MobiHoc'03, 2003, pp. 201–212.
- [4] J. Arias, Microprocessors and Microsystems, **28**(8), 403 (2004).
- [5] S.N. Simić, S. Sastry, "Distributed localization in wireless ad hoc networks," Tech. Report,

- UC Berkeley, 2002.
- [6] L. Doherty, L. E. Ghaoui, K. Pister, "Convex position estimation in wireless sensor networks" Proc. IEEE INFOCOM'01, 2001, pp. 1655–1663.
- [7] T. He, C.D. Huang, B.M. Blum, J.A. Stankovic, T. Abdelzaher, "Range-free localization schemes in large scale sensor networks," Proc. ACM MobiCom'03, 2003, pp. 81–95.
- [8] D. S. Li, M. Lei, J. Chen, and T. Sun. "Wireless sensor network positioning scheme with ring overlapping based on hybrid access of received signal strength indication," WiCOM'06, 2006, pp. 1–4.
- [9] P. Bahl and V.N. Padmanabhan, "RADAR: An in-building RF-based user location and tracking system," Proc. IEEE INFOCOM'00, 2000, pp. 775–784.
- [10] P. Biswas and Y. Ye, "Semidefinite programming for ad hoc wireless sensor network localization," IPSN '04, Apr. 2004.
- [11] N. Bulusu, J. Heidemann, and D. Estrin, "GPS-less Low Cost Outdoor Localization for Very Small Devices," IEEE Personal Communications Magazine, 2000.
- [12] D. Niculescu, B. Nath, "DV-based Positioning in Ad Hoc Networks," Journal of Telecommunication Systems, **22**(1/4), 267 (2003).
- [13] M. Sugano, "Indoor Localization System using RSSI Measurement of Wireless Sensor Network Based on Zigbee Standard," Wireless Sensor Network, 2006.
- [14] P. Barsocchi, "A Novel Approach to Indoor RSSI Localization by Automatic Calibration of the Wireless Propagation Model," Proc. IEEE VTC Spring 2009, 2009, pp. 1–5.
- [15] R. Stoleru, T. He, J.A. Stankovic, D. Luebke, "A high-accuracy, low-cost localization system for wireless sensor networks," Proc. 3rd International Conference on Embedded Networked Sensor Systems, 02–04 November 2005.
- [16] P. Chakraborty, "An Integrated Grid Portal for Managing Energy Resources," Third IEEE International Conference on e-Science and Grid Computing, 2007, pp. 25–33.
- [17] T. Parker, K. Langendoen, "Localisation in Mobile Anchor Networks," Technical Report PDS-2005-001, Delft Univ. of Technology, Feb. 2005.
- [18] L. Hu, D. Evans, "Localization for mobile sensor networks," Proc. ACM MobiCom'04, 2004, pp. 45–57.
- [19] N. Priyantha, H. Balakrishnan, E. Demaine, S. Teller, "Mobile-assisted localization in wireless sensor networks," Proc. IEEE INFOCOM'05, Mar. 2005.
- [20] Z. Y. Zhang, O. Berger, S. Sorbello, "A Cluster Based Approach Toward Sensor Localization and K-Coverage Problems," Ubiquitous Computing and Communication Journal, **2**(4), 15 (2007).
- [21] B. Xiao, H. K. Chen, S. G. Zhou, "Distributed Localization Using a Moving Beacon in Wireless Sensor Networks," IEEE Transactions on Parallel and Distributed systems, **19**, no.5, May 2008.

*Corresponding author: neu_mhb@163.com